International Journal of Solids and Structures 84 (2016) 99–109

Contents lists available at ScienceDirect

International Journal of Solids and Structures

journal homepage: www.elsevier.com/locate/ijsolstr

Elastic behavior of porous media with spherical nanovoids

Xavier Haller[a,c], Yann Monerie[b,c], Stéphane Pagano[b,c], Pierre-Guy Vincent[a,c,*]

[a] Institut de Radioprotection et de Sûreté Nucléaire, B.P. 3, 13115 Saint-Paul-lez-Durance Cedex, France
[b] Laboratoire de Mécanique et Génie Civil, Université de Montpellier, CNRS, CC 048 Place Eugène Bataillon, 34095 Montpellier Cedex, France
[c] Laboratoire de Micromécanique et Intégrité des Structures, IRSN-CNRS-UM, B.P. 3, 13115 Saint-Paul-lez-Durance Cedex, France

ARTICLE INFO

Article history:
Received 31 July 2015
Revised 11 January 2016
Available online 4 February 2016

Keywords:
Nanoporous materials
Spherical voids
Effective elastic properties
Micromechanical models
Morphologically representative pattern
Homogenization

ABSTRACT

This study is devoted to the effective elastic properties of nanoporous media containing spherical nanovoids. Nanocomposites materials are strongly dependent on their nanometric characteristic lengths. This size effect cannot be directly modeled using the classical homogenization schemes based on the Eshelby inclusion problem. However recent studies have extended the continuum mechanics and well-known micromechanical models to the nanoscale. In this paper, it is shown that these models can be replaced in a unified framework using the morphologically representative pattern-based approach of Stolz and Zaoui (1991) and therefore can be generalized to more complex microstructures. Following this approach, new bounds and estimates are derived. Two particular cases are treated: (i) the case of an ellipsoidal spatial distribution of the voids, (ii) the case of a biporous material containing both spherical nanovoids and randomly oriented spheroidal microvoids. The second case is typical of the microstructure of the irradiated uranium dioxide (UO_2). Thereby, the associated result could be used for determining the poro-elastic properties of these doubly voided materials.

1. Introduction

Nanoporous materials can be classified into the category of nanocomposites materials in which the characteristic length is typically of the order of a few nanometers (<100 nm, Paliwal and Cherkaoui (2012)). The particularity of this kind of materials is the high surface/volume ratio. Indeed, atoms near a surface are in a different local environment than those in the bulk: their coordination number is less than that of the bulk atoms and their energy is different (Duan et al., 2005a; 2005b; Paliwal and Cherkaoui, 2012; Wang et al., 2011). Therefore there is a disturbed region sometimes called the *interfacial region* whose thickness is of the order of few atomic layers (about one nanometer), which has a local elastic behavior different from that of the bulk (Paliwal and Cherkaoui, 2012; Wang et al., 2011). The impact of surfaces is often negligible in classical continuum mechanics but becomes predominant when the number of surface atoms is high as in nanocomposite materials (Brisard et al., 2010a; Duan et al., 2005a; 2005b; Le Quang and He, 2008; Paliwal and Cherkaoui, 2012; Wang et al., 2011). In particular, such surface effects have to be considered when deriving a model for the effective elastic behavior of these materials. The main consequence of the surface effects is a strong dependency of the effective properties to the nanometer characteristic length (Duan et al., 2005b; Paliwal and Cherkaoui, 2012; Sharma and Ganti, 2004). The present study is devoted to the modeling of the elastic properties of porous materials which exhibits cavities whose characteristic length is in the nanometer range.

Indeed, this is the case of the irradiated uranium dioxide (UO_2), which is commonly used as a nuclear fuel. The modeling of its mechanical behavior from up-scaling methods has recently motivated several studies (see for example Julien et al. (2011); Vincent et al. (2008); Vincent et al. (2009a, 2009b); Vincent et al. (2014a, 2014b)). This material contains intragranular cavities whose radii range between one and ten nanometers and pore density from 10^{23} m^{-3} to 10^{24} m^{-3} (Kashibe et al., 1993). Jelea et al. (2011) have carried out atomistic simulations and have determined the elastic moduli of a system built with periodic UO_2 elementary cells containing spherical nanocavities. Their results are compared to classical homogenization schemes in elasticity (Mori–Tanaka and self-consistent) and experimental data. Although there is a good agreement between the different results, it was shown that a surface effect exists at the scale of nanometric intragranular cavities in UO_2 and the results obtained from the homogenization approach could be improved by taking into account these surface effects.

* Corresponding author at: Institut de Radioprotection et de Sûreté Nucléaire, B.P. 3, 13115 Saint-Paul-lez-Durance Cedex, France. Tel.: +33 4 42 19 97 61; fax: +33 4 42 19 91 66.
E-mail addresses: xavier.haller@irsn.fr (X. Haller), yann.monerie@umontpellier.fr (Y. Monerie), stephane.pagano@umontpellier.fr (S. Pagano), pierre-guy.vincent@irsn.fr (P.-G. Vincent).

http://dx.doi.org/10.1016/j.ijsolstr.2016.01.018
0020-7683/

Description of the disturbed region. The first step to derive a micromechanical model with surface effects consists in giving a mechanical description to the disturbed region. There are mainly two ways to model this region. The first way is a zero thickness approach and the disturbed region is treated as an 'interface'. The interface stress model or 'imperfect coherent interface model' assumes that the traction vector is discontinuous across the surface and the displacement is continuous (Brisard et al., 2010a; 2010b; Duan et al., 2005a; 2005b; 2005c; 2006; 2007; Le Quang and He, 2008; Paliwal and Cherkaoui, 2012; Sharma and Ganti, 2004; Wang et al., 2005; 2011; 2007). This model is a limit case of a thin and stiff interphase (Wang et al., 2005) and is often used to model the disturbed region for nanocomposite materials.

The second way describes the disturbed region as an 'interphase' (Marcadon, 2005; Paliwal and Cherkaoui, 2012), i.e. as a classical three-dimensional coating. Although this approach is less used than the interface stress model, it makes no assumption concerning the stiffness and the thickness of the disturbed region. However it often leads to more complex analytical results.

Homogenization process. Once the description of the interfacial region is chosen, it has to be integrated in the homogenization process to derive models. Most of the classical micromechanical models are based on the Eshelby inclusion problem (Eshelby, 1957) and cannot deal with surface effects. Relatively recent works (Brisard et al., 2010a; 2010b; Duan et al., 2005b) have extended these classical models to the case of nanocomposite materials, particularly the Hashin (1962) composite sphere assemblage model, the Mori and Tanaka (1973) model, and the generalized self-consistent model (Christensen and Lo, 1979). These models, developed by analogy with their classical counterparts, are based on a *modified* inclusion problem in which the perfect interface[1] between the spherical inclusion and the surrounding medium is replaced by an imperfect coherent interface (as stated above, the term *coherent* means that the displacement field is continuous across the interface). The solving of this problem generally leads to non-uniform deformation fields inside the inclusion. This generalization of the classical results is limited to the case of materials containing nanospherical inclusions isotropically distributed inside the bulk. However, it is shown in the sequel that they can be derived in the theoretical framework of the morphologically representative pattern (MRP) theory (Bornert, 1996a; 1996b; 2001; Bornert et al., 1996; Stolz and Zaoui, 1991) and thus extended to the case of materials with more complex microstructures such as an ellipsoidal spatial distribution of voids.

Morphologically representative pattern. The MRP theory extends the classical approach: it allows us to take some finer details of the microstructure into account and particularly the local arrangement of the phases. It is convenient in the case of nanoparticulate composites (also called materials with an inclusion-matrix morphology[2]), in which the disturbed region is included between the matrix and the heterogeneities and locally perturbs the mechanical fields. The establishment of the effective elastic moduli through this approach requires the solving of auxiliary problems related to heterogeneous inclusions embedded in an infinite medium. In the case of the spherical inclusions or voids, these auxiliary problems are similar to those solved by Duan et al. (2005b) and correspond to a single spherical inclusion coated with a disturbed region (modeled as an interface or an interphase) surrounded by a matrix phase. It is shown here that the MRP approach delivers a better understanding concerning the assumptions underlying in the already existing models.

[1] A perfect interface (or a perfect bonding condition) means that the traction vector and the displacement are continuous across two adjacent media.

[2] The material is made of a predominant phase in which heterogeneities (inclusions, voids or *heterogeneous* inclusions) are included.

The present study is organized as follows. The interface stress model typically used for nanomaterials is shortly described in Section 2. In Section 3, the theory and the main results concerning the MRP approach are summarized. This section is also devoted to a direct use of the MRP theory in the case of nanoporous materials and it is shown that the existing models can be directly derived from the MRP approach. Section 4 deals with some original results, corresponding to particular cases that can be easily treated following the MRP theory. It illustrates the ability of the MRP approach to catch the effective elastic properties of materials containing nanospherical voids. Two particular cases are discussed in this section: (i) spheroidal spatial distributions of voids, (ii) a biporous medium containing spherical nanovoids together with larger spheroidal voids. The second case is typical of the microstructure of irradiated UO_2 and the results are then plotted with characteristic moduli for this material.

2. Nanomaterials: modeling of the disturbed region with the interface stress model

As already stated, the interface stress model is intensively used in the case of nanomaterials. It assumes a traction vector jump across the interface whereas the displacement is continuous. This model has been proposed by Gurtin and Murdoch (1975) developing a theoretical framework for the mechanical behavior of material surfaces.

The Gurtin and Murdoch model consists in a set of two equations: a surface constitutive law and a balance equation. The surface constitutive law is assumed to be composed of two parts: a surface internal stress, called by analogy with liquids a 'surface tension', which is independent on the external loading and an elastic part whose moduli are distinct from those of the bulk. The elastic behavior is often assumed to remain isotropic in the tangent plane. For polycristals with intragranular nanocavities, such as the irradiated UO_2, due to the crystal anisotropy, the mechanical behavior of the disturbed region around each cavity is probably not isotropic. It is unlikely that the disturbed region is in a particular crystallographic orientation and it is certainly randomly oriented. Although the hypothesis of an isotropic elastic behavior of the disturbed region is not really equivalent to the case of randomly oriented disturbed regions, the complexity generated by anisotropy to develop non-numerical micromechanical models would be higher than the gain of precision by taking account of it (Duan et al., 2005b; Paliwal and Cherkaoui, 2012). As a result, the elastic behavior of the surface is commonly considered as isotropic.

The surface between two media (1 and 2) is denoted by Γ. The unit normal vector to Γ (oriented from 1 to 2) is denoted by $\boldsymbol{n}$ and the two vectors $\boldsymbol{t}_t$ and $\boldsymbol{t}_b$ are unit vectors contained in the tangent plane to Γ. These three vectors are assumed to be pairwise orthogonal and $(\boldsymbol{t}_t, \boldsymbol{t}_b, \boldsymbol{n})$ forms a vector basis for 3 dimensional vectors ($\boldsymbol{n} = \boldsymbol{t}_t \wedge \boldsymbol{t}_b$). The couple $(\boldsymbol{t}_t,\ \boldsymbol{t}_b)$ is a basis for surface tangent vectors. The second-order identity tensor in the tangent plane $\boldsymbol{i}_T$ and the fourth-order identity tensor in the tangent plane $\mathbb{I}_T$ are defined as:

$$\boldsymbol{i}_T = \boldsymbol{i} - \boldsymbol{n} \otimes \boldsymbol{n} \tag{1}$$

$$\mathbb{I}_T = \sum_{\alpha,\beta=t,b} \Big[\boldsymbol{t}_\alpha \otimes \boldsymbol{t}_\alpha \otimes \boldsymbol{t}_\alpha \otimes \boldsymbol{t}_\alpha + \frac{1}{2}\left(\boldsymbol{t}_\alpha \otimes \boldsymbol{t}_\beta \otimes \boldsymbol{t}_\alpha \otimes \boldsymbol{t}_\beta + \boldsymbol{t}_\alpha \otimes \boldsymbol{t}_\beta \otimes \boldsymbol{t}_\beta \otimes \boldsymbol{t}_\alpha\right) \Big] \tag{2}$$

where $\boldsymbol{i}$ is the classical second-order identity tensor ($i_{kl} = 1$ if $k = l$, $i_{kl} = 0$ otherwise) and $\otimes$ denotes the tensor product. The two tensors $\boldsymbol{i}_T$ and $\mathbb{I}_T$ can be seen as projectors onto the surface, in the sense that they serve to extract the tangential parts of vectors or

second-order tensors. The surface constitutive relation which expresses the surface stress $\boldsymbol{\sigma}_s$ in terms of the surface strain $\boldsymbol{\epsilon}_s$ can be written in the infinitesimal strain framework as follows (Huang and Wang, 2006; Ru, 2010):

$$\boldsymbol{\sigma}_s = \tau_s \boldsymbol{i}_T + \mathbb{C}_s : \boldsymbol{\epsilon}_s \tag{3}$$

$$\mathbb{C}_s = 2(k_s \mathbb{J}_T + \mu_s \mathbb{K}_T) \tag{4}$$

The tensors $\mathbb{J}_T = (1/2)(\boldsymbol{i}_T \otimes \boldsymbol{i}_T)$ and $\mathbb{K}_T = \mathbb{I}_T - \mathbb{J}_T$ are two tensors among the six classical tensors for the transversely isotropic basis of the fourth-order tensors. They are projectors in the sense that if $\boldsymbol{\epsilon}$ is a strain tensor, then the non-zero components of $\mathbb{K}_T : \boldsymbol{\epsilon}$ are only the transverse shear strains and $\mathbb{J}_T : \boldsymbol{\epsilon}$ expresses the section changing in the tangent plane. The surface elastic moduli have unusual dimensions. Indeed, they have the dimension of a force per unit length (N/m). This paper is devoted to the modeling of the effective elastic moduli. The influence of the surface tension, denoted by τ_s in Eq. (3), on the overall mechanical behavior is not investigated in this article (τ_s is set to zero in the sequel).

The surface strain $\boldsymbol{\epsilon}_s$ corresponds to the tangential part of the strain in the matrix or in the inclusion at the interface and is determined from:

$$\boldsymbol{\epsilon}_s(\boldsymbol{x}) = \mathbb{I}_T : \boldsymbol{\epsilon}_1(\boldsymbol{x}) = \mathbb{I}_T : \boldsymbol{\epsilon}_2(\boldsymbol{x}), \quad \forall \boldsymbol{x} \in \Gamma \tag{5}$$

Concerning the balance equation, the most commonly used equation is the Generalized Young Laplace equation. This equation links the stress jump at the interface $[\boldsymbol{\sigma}] = \boldsymbol{\sigma}_2(\boldsymbol{x}) - \boldsymbol{\sigma}_1(\boldsymbol{x}), \ \forall \boldsymbol{x} \in \Gamma$ to the surface stress $\boldsymbol{\sigma}_s$ and to the second-order curvature tensor $\boldsymbol{b}$ (Brisard et al., 2010a; 2010b) :

$$[\boldsymbol{\sigma}] \cdot \boldsymbol{n} + (\boldsymbol{\sigma}_s : \boldsymbol{b})\boldsymbol{n} + \mathrm{div}_s \boldsymbol{\sigma}_s = \boldsymbol{0} \tag{6}$$

Here, the operator div_s refers to as the surface divergence of the two-dimensional second-order tensors.

3. MRP-based approach

3.1. General framework

The MRP-based approach was first proposed by Stolz and Zaoui (1991) and then followed by Bornert (1996a); 1996b); 2001); Bornert et al. (1996). It considers non uniform admissible elastic fields over the phases on the heterogeneous material. This approach allows us to take into account some details on the microstructure, especially the relative local phases arrangement. As a consequence, it allows us to introduce some characteristic lengths in the micromechanical models. This approach is used by Marcadon (2005) to derive the effective elastic properties of nanocomposite materials with randomly distributed spherical inclusions. In Marcadon (2005), the disturbed region is modeled as an interphase. On the other hand, Brisard et al. (2010b) also use the MRP concept to derive a Mori–Tanaka-like estimate for the shear modulus of a nanomaterial with randomly distributed spherical inclusions (which becomes a bound under certain conditions).

The MRP approach assumes that the representative volume element (RVE) can be split into separated subdomains. These subdomains are grouped together into families called morphologically representative patterns. All the members of a pattern exhibits the same geometry and the same spatial distribution of the mechanical properties. The heterogenous medium is then characterized by the description of all its patterns and the positions of all their members inside the volume as illustrated in Fig. 1. The patterns are described as *morphologically representative* by Bornert et al. (1996) since they take into account some primary morphological characteristics of the heterogeneous material such as the phase continuity or discontinuity, the presence of inclusions in a surrounding material, the shapes and the orientations of the inclusions.

Here, the domain occupied by the RVE is denoted by Ω. This domain can be split into p patterns (subscript $r \in [1, \ldots, p]$) and a surrounding matrix. Each pattern has N_r members. The members (superscript i) of each pattern r are defined over their domains D_r^i centered at the points $\boldsymbol{x}_r^i$ ($\forall r \in [1, \ldots, p]$ and $\forall i \in [1, \ldots, N_r]$).

The domains D_r ($\forall r \in [1, \ldots, p]$) are centered at the origin and are such that the domains D_r^i are obtained from the domains D_r by a translation of $\boldsymbol{x}_r^i$. So a pattern is characterized by a given domain D_r and a spatial distribution of local elastic moduli $\mathbb{C}_r(\boldsymbol{u})$ ($\forall \boldsymbol{u} \in D_r$).

While the domains D_r and the distributions of the local elastic moduli $\mathbb{C}_r$ are assumed to be given data, only statistical information on the characteristic functions are available. The first and second order informations, respectively the volume fractions and the correlation functions[3], are supposed to be known. This paper is devoted to the particular case of an ellipsoidal distribution of the centers.

The total domain Ω is not necessarily described by the patterns only. A domain D_m can subsist around the patterns: an homogeneous matrix phase surrounding all the patterns can be considered and it is called *the Matrix Outside the Patterns (MOP)* in the sequel: the subscript associated to this domain is m. Its elastic stiffness tensor is denoted by $\mathbb{C}_m$ and c_m denotes its volume fraction.

The overall stress and strain are defined as the volume averages of the local stress and strain fields over the RVE:

$$\bar{\boldsymbol{\sigma}} = \frac{1}{|\Omega|}\int_\Omega \boldsymbol{\sigma}(\boldsymbol{x})\, d\boldsymbol{x}, \quad \bar{\boldsymbol{\epsilon}} = \frac{1}{|\Omega|}\int_\Omega \boldsymbol{\epsilon}(\boldsymbol{x})\, d\boldsymbol{x}. \tag{7}$$

The averages of the stress and the strain over the domain D_r are respectively denoted by $\langle \boldsymbol{\sigma} \rangle_{D_r}$ and $\langle \boldsymbol{\epsilon} \rangle_{D_r}$:

$$\langle \boldsymbol{\sigma} \rangle_{D_r} = \frac{1}{|D_r|}\int_{D_r} \boldsymbol{\sigma}(\boldsymbol{x})\, d\boldsymbol{x}, \quad \langle \boldsymbol{\epsilon} \rangle_{D_r} = \frac{1}{|D_r|}\int_{D_r} \boldsymbol{\epsilon}(\boldsymbol{x})\, d\boldsymbol{x}. \tag{8}$$

From the MRP-based description, different kinds of models can be derived. These models contain distinct morphological informations. First-order bounds can be derived. The upper bound is called the Generalized Voigt (GV) bound and is expressed as follows:

$$\mathbb{C}_{\mathrm{M}}^{\mathrm{GV}} = c_m \mathbb{C}_m + \sum_{r=1}^{p} c_r \mathbb{C}_{\mathrm{Mr}}^{\mathrm{GV}} \quad \text{with} \quad \langle \mathbb{C}_r : \boldsymbol{\epsilon} \rangle_{D_r} = \mathbb{C}_{\mathrm{Mr}}^{\mathrm{GV}} : \bar{\boldsymbol{\epsilon}}, \quad \forall\, \bar{\boldsymbol{\epsilon}} \tag{9}$$

The lower bound, called the Generalized Reuss (GR) bound, is expressed as follows:

$$\left(\mathbb{C}_{\mathrm{M}}^{\mathrm{GR}}\right)^{-1} = c_m (\mathbb{C}_m)^{-1} + \sum_{r=1}^{p} c_r \left(\mathbb{C}_{\mathrm{Mr}}^{\mathrm{GR}}\right)^{-1}$$
$$\text{with} \quad \left\langle (\mathbb{C}_r)^{-1} : \boldsymbol{\sigma} \right\rangle_{D_r} = \left(\mathbb{C}_{\mathrm{Mr}}^{\mathrm{GR}}\right)^{-1} : \bar{\boldsymbol{\sigma}}, \quad \forall\, \bar{\boldsymbol{\sigma}} \tag{10}$$

The tensors $\mathbb{C}_{\mathrm{Mr}}^{\mathrm{GV}}$ and $\mathbb{C}_{\mathrm{Mr}}^{\mathrm{GR}}$ are the overall stiffness tensors obtained from the study of a single pattern r subjected to the macroscopic strain $\bar{\boldsymbol{\epsilon}}$ (for $\mathbb{C}_{\mathrm{Mr}}^{\mathrm{GV}}$) or to the macroscopic stress (for $\mathbb{C}_{\mathrm{Mr}}^{\mathrm{GR}}$) $\bar{\boldsymbol{\sigma}}$ on its boundary. It corresponds to a Generalized Hashin assemblage of pattern r subjected to $\bar{\boldsymbol{\epsilon}}$ or $\bar{\boldsymbol{\sigma}}$ at infinity (Bornert, 2001).

As in the classical approach, the previous bounds can be improved by adding informations on the spatial distribution of the centers of the patterns. A procedure inspired of the classical Hashin and Shtrikman variational formulation has been derived in the MRP context and lead to second-order bounds or estimates. As already stated, the spatial distribution of the centers of the patterns is assumed to be ellipsoidal. For the three cases presented herefater, Bornert (2001) shows that the optimal polarization fields

[3] In the present paper, the correlation functions p_{rs} have the following form: $\forall (r,s) \in [1,p]^2 \quad \forall \boldsymbol{h} \neq \boldsymbol{0} \quad p_{rs}(\boldsymbol{h}) = \psi_{rs}(||\boldsymbol{\alpha} : \boldsymbol{h}||)$ where $\boldsymbol{\alpha}$ is a second-order symmetric normalized tensor and ψ_{rs} a scalar function with scalar arguments. The case $\boldsymbol{\alpha} = \boldsymbol{i}$ corresponds to the isotropic case.

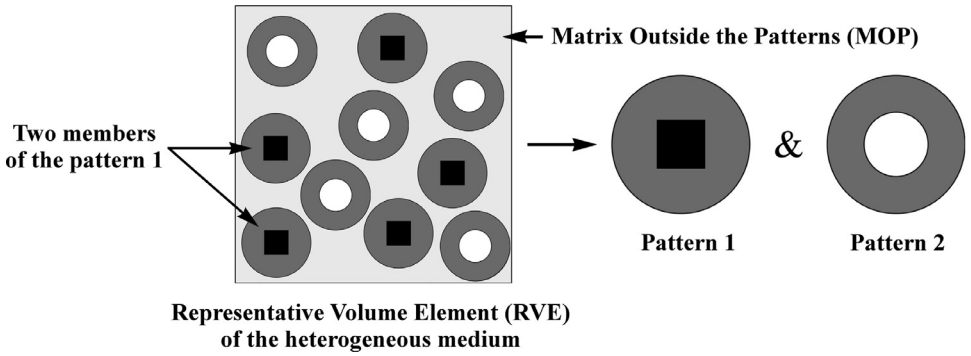

Fig. 1. Schematic illustration of the MRP approach: particular case of a decomposition of the RVE using two patterns (whose the external shape is spherical) and a surrounding matrix.

are obtained by solving $p+1$ auxiliary problems. Each problem is relative to an inclusion (made by a single pattern or by the MOP) embedded in an infinite medium. The infinite medium, also called the reference medium, is indexed by 0 and its elastic stiffness tensor is denoted by $\mathbb{C}_0$. A remote strain $\boldsymbol{\epsilon}^0$ is applied at infinity. The mean polarization field over the domain D_r $\langle\boldsymbol{\tau}\rangle_{D_r}$ is defined as $\langle\boldsymbol{\sigma}\rangle_{D_r} - \mathbb{C}_0 : \langle\boldsymbol{\epsilon}\rangle_{D_r}$. Then a tensor $\mathbb{T}^0_{\mathrm{Mr}}$ is introduced for each auxiliary problem:

$$\langle\boldsymbol{\tau}\rangle_{D_r} = \mathbb{T}^0_{\mathrm{Mr}} : \boldsymbol{\epsilon}^0 \tag{11}$$

Again, each auxiliary problem can be seen as a problem of a generalized Hashin assemblage where the overall strain is equal to the mean strain over the pattern. The fourth-order tensor linking $\langle\boldsymbol{\sigma}\rangle_{D_r}$ and $\langle\boldsymbol{\epsilon}\rangle_{D_r}$ is thus commonly denoted by $\mathbb{C}^{\mathrm{HS}}_{\mathrm{Mr}}(\mathbb{C}^0)$:

$$\langle\boldsymbol{\sigma}\rangle_{D_r} = \mathbb{C}^{\mathrm{HS}}_{\mathrm{Mr}}(\mathbb{C}_0) : \langle\boldsymbol{\epsilon}\rangle_{D_r} \tag{12}$$

Moreover, one should remark that the previous tensors $\mathbb{C}^{\mathrm{GV}}_{\mathrm{Mr}}$ and $\mathbb{C}^{\mathrm{GR}}_{\mathrm{Mr}}$ can be determined from the tensor $\mathbb{C}^{\mathrm{HS}}_{\mathrm{Mr}}(\mathbb{C}_0)$ as follows:

$$\lim_{\|\mathbb{C}_0\|\to+\infty} \mathbb{C}^{\mathrm{HS}}_{\mathrm{Mr}}(\mathbb{C}_0) = \mathbb{C}^{\mathrm{GV}}_{\mathrm{Mr}}, \qquad \lim_{\|\mathbb{C}_0\|\to 0} \mathbb{C}^{\mathrm{HS}}_{\mathrm{Mr}}(\mathbb{C}_0) = \mathbb{C}^{\mathrm{GR}}_{\mathrm{Mr}} \tag{13}$$

where $\|.\|$ denotes a norm for the fourth order symmetric tensors. Indeed, when $\mathbb{C}_0$ tends to the rigid case, an homogeneous strain is applied on the boundary of the pattern and when $\mathbb{C}_0$ tends to the porous case, an homogeneous stress is applied on its boundary.

Following Bornert (1996b), three particular cases are considered here. In the first case (*case 1*), the reference medium has the same elastic properties as the matrix. This model is called the Mori–Tanaka-type model or the Generalized Mori–Tanaka model (GMT). In the second case (*case 2*), the volume fraction of matrix which is not included inside the patterns (the MOP) is equal to zero. The tessellation of the RVE consists in a Hashin-like assemblage. Such a material is called a Generalized Hashin assemblage. To build such an assemblage, the following conditions have to be checked:

- the patterns have all the same ellipsoidal external shape (same aspect ratio and same orientation) and this shape is related to the spatial distribution of the centers of the patterns,
- the assemblage is fractal and so the patterns cannot have a well definite size.

In this second case, the choice for the reference medium remains free. In the third case (*case 3*), the external shape of the patterns is related to the spatial distribution of the centers of the patterns (as in the previous case). So the patterns have all the same ellipsoidal external shape. But unlike the previous case, the volume fraction of the matrix which is not included in the patterns is not necessarily equal to zero. In this case, the MOP can be treated as an additional homogeneous pattern. For these three specific cases, the effective stiffness tensor can be written as:

Case 1:

$$\mathbb{C}^{\mathrm{GMT}}_{\mathrm{M}} = \mathbb{C}_m + \left(\mathbb{I} - \langle\mathbb{T}^m_{\mathrm{Mr}}\rangle_{\mathrm{M}} : \mathbb{P}^m_d\right)^{-1} : \langle\mathbb{T}^m_{\mathrm{Mr}}\rangle_{\mathrm{M}} \tag{14}$$

In this expression, the operator $\langle.\rangle_{\mathrm{M}}$ is defined as the average $\langle\mathbb{X}\rangle_{\mathrm{M}} = \sum_{r=1}^{p} c_r\mathbb{X}_r$ and $\mathbb{I}$ is the classical fourth-order identity tensor. The tensor $\mathbb{P}^0_d$ is the Hill tensor related to the ellipsoidal spatial distribution of the centers of the patterns and to the stiffness tensor of the reference medium $\mathbb{C}_0$. The Hill tensor $\mathbb{P}(\mathbb{C}_0)$ is related to the Eshelby tensor $\mathbb{S}^E(\mathbb{C}_0)$:

$$\mathbb{P}(\mathbb{C}_0) = \mathbb{S}^E(\mathbb{C}_0) : \mathbb{C}_0^{-1} \tag{15}$$

Case 2 ($c_m = 0$):

$$\mathbb{C}^{\mathrm{HS}}_{\mathrm{M}}(\mathbb{C}_0) = \mathbb{C}_0 + \left(\mathbb{I} - \left\langle\mathbb{T}^0_{\mathrm{Mr}}\right\rangle_{\mathrm{M}} : \mathbb{P}^0_d\right)^{-1} : \left\langle\mathbb{T}^0_{\mathrm{Mr}}\right\rangle_{\mathrm{M}} \tag{16}$$

Case 3: Here the MOP can then be seen as an additional homogeneous pattern. Its auxiliary problem consists in an homogeneous inclusion with stiffness $\mathbb{C}_m$ and with the same shape as the patterns. This inclusion is embedded in an infinite medium with stiffness $\mathbb{C}_0$ subjected to a remote strain $\boldsymbol{\epsilon}^0$ at infinity. As in expression (11), a tensor $\mathbb{T}^0_m$ can be introduced such that: $\langle\boldsymbol{\tau}\rangle_{D_m} = \mathbb{T}^0_m : \boldsymbol{\epsilon}^0$. In this case:

$$\mathbb{C}^{\mathrm{HS}}_{\mathrm{M}}(\mathbb{C}_0) = \mathbb{C}_0 + \left(\mathbb{I} - \left\langle\mathbb{T}^0_{\mathrm{Mr}}\right\rangle_{\mathrm{M}} : \mathbb{P}^0_d - c_m\mathbb{T}^0_m : \mathbb{P}^0_d\right)^{-1} : \left(\left\langle\mathbb{T}^0_{\mathrm{Mr}}\right\rangle_{\mathrm{M}} + c_m\mathbb{T}^0_m\right) \tag{17}$$

If the patterns have the same shape as the spatial distribution of their centers (cases 2 and 3 always meet this condition), then (inequality in the sense of the quadratic forms):

$$\mathbb{C}^{\mathrm{GR}}_{\mathrm{M}} < \mathbb{C}^{\mathrm{HS}}_{\mathrm{M}}(\mathbb{C}_0) < \mathbb{C}^{\mathrm{GV}}_{\mathrm{M}} \tag{18}$$

Unlike case 1, cases 2 and 3 allow an arbitrary reference medium. The specific choice $\mathbb{C}_0 = \mathbb{C}^{\mathrm{HS}}_{\mathrm{M}}(\mathbb{C}_0)$ lead to a self-consistent model called the Generalized Self-Consistent model (GSC).

3.2. Auxiliary problem for spherical nanovoids with interface stress model

The objective is to apply the MRP approach to the case of a porous material with spherical nanovoids. Here, the auxiliary problem of a pattern made by a spherical cavity (index v) embedded in a matrix layer (index m) is considered. At the interface between the cavity and the matrix, the disturbed region is taken into account by using the interface stress model. This pattern is denoted by $\mathcal{S}$. The outer shape of the pattern is chosen spherical and concentric with respect to the cavity. The center of the pattern is defined as the center of the cavity. The radius of the cavity and the external radius of the pattern are respectively denoted by r_1 and r_0.

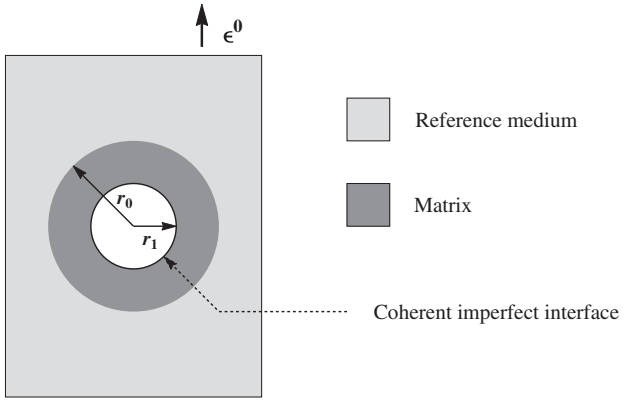

Fig. 2. Problem of the heterogeneous inclusion in an infinite reference medium for spherical nanovoids with the interface stress model.

The porosity of the pattern $\mathcal{S}$, denoted by $f_{\mathcal{S}}$, is equal to $(r_1/r_0)^3$. The surfaces Γ_1 and Γ_0 are respectively characterized by $r = r_1$ and $r = r_0$ in the classical spherical coordinates system.

The study is limited to the case of an ellipsoidal spatial distribution of the centers of the voids. Following the MRP approach, auxiliary problems are defined as heterogeneous inclusions (with the same microstructures as the patterns) which are embedded in an infinite homogeneous medium (called the reference medium and denoted by 0) submitted to a remote strain $\boldsymbol{\epsilon}^0$ applied at infinity. This problem is illustrated in Fig. 2. Hereafter, the domain occupied by a phase i is denoted by ω_i. The set of equations reads as follows ($\boldsymbol{u}$ refers to a displacement field and $\boldsymbol{\epsilon}$ is the linearized strain tensor):

$$\begin{cases} \mathrm{div}\boldsymbol{\sigma} = \boldsymbol{0}, \quad \boldsymbol{\epsilon} = \dfrac{1}{2}\left(\mathrm{grad}\boldsymbol{u} + {}^{\mathrm{T}}\mathrm{grad}\boldsymbol{u}\right) \text{ in } \omega_0 \text{ and } \omega_m \\ \boldsymbol{\sigma} = \mathbb{C}_0 : \boldsymbol{\epsilon} \text{ in } \omega_0 \text{ and } \boldsymbol{\sigma} = \mathbb{C}_m : \boldsymbol{\epsilon} \text{ in } \omega_m \\ \left(\boldsymbol{\sigma}^{(0)} - \boldsymbol{\sigma}^{(m)}\right)\cdot\boldsymbol{n} = \boldsymbol{0} \text{ and } \left(\boldsymbol{u}^{(0)} - \boldsymbol{u}^{(m)}\right) = \boldsymbol{0} \quad \text{on } \Gamma_0 \\ \left(\boldsymbol{\sigma}^{(m)} - \boldsymbol{\sigma}^{(v)}\right)\cdot\boldsymbol{n} + (\boldsymbol{\sigma}_s : \boldsymbol{b})\boldsymbol{n} + \mathrm{div}_s\boldsymbol{\sigma}_s = \boldsymbol{0}, \quad \boldsymbol{\epsilon}_s = \mathbb{I}_T : \boldsymbol{\epsilon}, \\ \qquad \boldsymbol{\sigma}_s = \mathbb{C}_s : \boldsymbol{\epsilon}_s \quad \text{on } \Gamma_1 \\ \boldsymbol{\sigma} = \boldsymbol{0} \quad \text{in } \omega_v \text{ and } \boldsymbol{u} = \boldsymbol{\epsilon}^0\cdot\boldsymbol{x} \text{ when } ||\boldsymbol{x}|| \to \infty \end{cases} \tag{19}$$

where $\boldsymbol{\sigma}^{(0)}$, $\boldsymbol{\sigma}^{(m)}$, and $\boldsymbol{\sigma}^{(v)}$ denote the stress tensors respectively in the infinite medium, in the matrix, and in the void. The vectors $\boldsymbol{u}^{(0)}$, $\boldsymbol{u}^{(m)}$, and $\boldsymbol{u}^{(v)}$ denote the displacement vectors respectively in the infinite medium, in the matrix, and in the void. The vector $\boldsymbol{n}$ denotes the unit normal vector to Γ_i ($\forall i \in \{0, 1\}$) oriented to the matrix.

The elastic behaviors of the matrix and the reference medium are assumed to be isotropic ($\mathbb{J} = 1/3(\boldsymbol{i}\otimes\boldsymbol{i})$, $\mathbb{K} = \mathbb{I} - \mathbb{J}$):

$$\mathbb{C}_m = 3k_m\mathbb{J} + 2\mu_m\mathbb{K} \quad \text{and} \quad \mathbb{C}_0 = 3k_0\mathbb{J} + 2\mu_0\mathbb{K} \tag{20}$$

The surface elastic tensor is specified in Eq. (4). The determining of the fourth-order tensor $\mathbb{T}^0_{\mathrm{M}\mathcal{S}}$ and $\mathbb{C}^{\mathrm{HS}}_{\mathrm{M}\mathcal{S}}$ is given in Appendix A by solving the problem (19). Due to the spherical symmetry and to the isotropic behaviors of the phases, these tensors are isotropic and they can be written as follows:

$$\mathbb{T}^0_{\mathrm{M}\mathcal{S}} = T^0_{\mathrm{M}\mathcal{S}|h}\mathbb{J} + T^0_{\mathrm{M}\mathcal{S}|d}\mathbb{K}, \quad \mathbb{C}^{\mathrm{HS}}_{\mathrm{M}\mathcal{S}} = 3k^{\mathrm{HS}}_{\mathrm{M}\mathcal{S}}\mathbb{J} + 2\mu^{\mathrm{HS}}_{\mathrm{M}\mathcal{S}}\mathbb{K} \tag{21}$$

where $T^0_{\mathrm{M}\mathcal{S}|h}$, $k^{\mathrm{HS}}_{\mathrm{M}\mathcal{S}}$ are given in (A.2), and $T^0_{\mathrm{M}\mathcal{S}|d}$, $\mu^{\mathrm{HS}}_{\mathrm{M}\mathcal{S}}$ are given in (A.8).

Unlike the effective bulk modulus $k^{\mathrm{HS}}_{\mathrm{M}\mathcal{S}}$, the shear modulus $\mu^{\mathrm{HS}}_{\mathrm{M}\mathcal{S}}$ depends on the stiffness $\mathbb{C}_0$ (to be more precise it depends only on the shear modulus μ_0). Following (13), the tensors $\mathbb{C}^{\mathrm{GV}}_{\mathrm{M}\mathcal{S}}$ and $\mathbb{C}^{\mathrm{GR}}_{\mathrm{M}\mathcal{S}}$ are obtained:

$$\mathbb{C}^{\mathrm{GV}}_{\mathrm{M}\mathcal{S}} = 3k^{\mathrm{HS}}_{\mathrm{M}\mathcal{S}}\mathbb{J} + 2\mu^{\mathrm{GV}}_{\mathrm{M}\mathcal{S}}\mathbb{K}, \quad \mathbb{C}^{\mathrm{GR}}_{\mathrm{M}\mathcal{S}} = 3k^{\mathrm{HS}}_{\mathrm{M}\mathcal{S}}\mathbb{J} + 2\mu^{\mathrm{GR}}_{\mathrm{M}\mathcal{S}}\mathbb{K} \tag{22}$$

The shear moduli $\mu^V_{\mathrm{M}\mathcal{S}}$ and $\mu^R_{\mathrm{M}\mathcal{S}}$ are given in (A.15). They will be used after to derive the GV and GR bounds according to Eqs. (9) and (10).

3.3. Particular cases derived from the MRP approach

In this section, some particular cases derived from the generalized estimates and bounds and based on the pattern $\mathcal{S}$ are treated. By the way, it is shown how the already existing models for nanoporous media can be replaced into the framework of the MRP approach.

3.3.1. GMT estimates

In the case of the GMT models, the reference medium has the same elastic properties as the matrix. Therefore the polarization fields over the MOP and in the matrix phases included inside the patterns vanish. It implies that the external shape and the external length of the patterns have no influence on the overall properties evaluated with this kind of models. Then the external shape of the patterns are not necessarily related to the spatial distribution of the centers, unlike other models (such as the GSC estimate, the GV and GR bounds). The external radii of the patterns characterizing the distance between the centers of the patterns, the packing effects cannot be taken into account. In this case, the tensor $\mathbb{T}^m_{\mathrm{M}\mathcal{S}}$ used to derive the GMT estimates for the effective moduli (Eq. (14)) is expressed as:

$$\mathbb{T}^m_{\mathrm{M}\mathcal{S}} = T^m_{\mathrm{M}\mathcal{S}|h}\mathbb{J} + T^m_{\mathrm{M}\mathcal{S}|d}\mathbb{K} \tag{23}$$

where $T^m_{\mathrm{M}\mathcal{S}|h}$ and $T^m_{\mathrm{M}\mathcal{S}|d}$ are respectively specified in (A.4) and (A.16).

If the interface is rigid (i.e. k_s and μ_s tend to infinity) or if the radius r_1 of the void is equal to zero, then the tensor $\mathbb{T}^m_{\mathrm{M}\mathcal{S}}$ reduces to (with $f_{\mathcal{S}} = 1$, it means that there is no matrix phase inside the pattern $\mathcal{S}$):

$$\mathbb{T}^m_{\mathrm{M}\mathcal{S}} = (3k_m + 4\mu_m)\mathbb{J} + \frac{5\mu_m(3k_m + 4\mu_m)}{3(k_m + 2\mu_m)}\mathbb{K} \tag{24}$$

On the other hand, if the interface is soft (i.e. k_s and μ_s are vanishing) or if the radius r_1 of the void tends to infinity, then its expression reduces to (with $f_{\mathcal{S}} = 1$):

$$\mathbb{T}^m_{\mathrm{M}\mathcal{S}} = -\frac{3k_m(3k_m + 4\mu_m)}{4\mu_m}\mathbb{J} - \frac{10\mu_m(3k_m + 4\mu_m)}{9k_m + 8\mu_m}\mathbb{K} \tag{25}$$

The two previous expressions correspond to the classical tensors $\mathbb{T}^m_i$ without surface effect, corresponding respectively to rigid inclusions and to pores. In other words:

- when the interface is very stiff or when the radius of the void r_1 tends to zero, the medium behaves as if the cavities were replaced by stiff inclusions,
- when the interface is infinitely soft or when the radius tends to infinity, the surface effect becomes negligible and the medium behaves as a classical porous medium without surface effect.

When the medium contains a single pattern $\mathcal{S}$, the effective stiffness tensor related to the GMT scheme is expressed as follows:

$$\mathbb{C}^{\mathrm{GMT}}_{\mathrm{M}} = \mathbb{C}_m + (\mathbb{I} - c_{\mathcal{S}}\mathbb{T}^m_{\mathrm{M}\mathcal{S}} : \mathbb{P}^m_d)^{-1} : c_{\mathcal{S}}\mathbb{T}^m_{\mathrm{M}\mathcal{S}} \tag{26}$$

where $c_{\mathcal{S}}$ is the volume fraction of the pattern $\mathcal{S}$ in the RVE. Then, the total porosity over the RVE, denoted by f in the sequel, is equal to $f_{\mathcal{S}}\, c_{\mathcal{S}}$. This result shows that the tensor $\mathbb{C}^{\mathrm{GMT}}_{\mathrm{M}}$ depends on $f_{\mathcal{S}}$ and $c_{\mathcal{S}}$ only through the total porosity f. Again, it means that the overall properties evaluated with this model do not depend on the external radius r_0 of the pattern $\mathcal{S}$.

In the particular case of an isotropic spatial distribution of the centers of the pattern $\mathcal{S}$, this expression leads to the following bulk and shear moduli:

$$k_{\mathrm{M}}^{\mathrm{GMT}} = k_m + \frac{f}{3}\frac{(3k_m+4\mu_m)(4k_s-3k_m r_1)}{4(1-f)k_s + r_1(3fk_m+4\mu_m)} \tag{27}$$

$$\mu_{\mathrm{M}}^{\mathrm{GMT}} = \mu_m + f\frac{5\beta_d\mu_m(3k_m+4\mu_m)}{3k_m\delta_d + 4\mu_m\zeta_d - 6f\beta_d(k_m+2\mu_m)} \tag{28}$$

where β_d, δ_d, and ζ_d are given in (A.16). Therefore the effective moduli are equal to those already established by Duan et al. (2005b).

From this, an ellipsoidal spatial distribution of the centers can be easily taken into account using the adapted expression of $\mathbb{P}_d^m$. The influence of the spatial distribution of the centers of the pattern $\mathcal{S}$ on the effective elastic properties will be investigated in Section 4.1.

3.3.2. Other bounds and estimates

The self-consistent model of Duan et al. (2005b) can also be directly refound by using the expressions (17), (21), (A.2), and (A.8) together with $\mathbb{C}_0 = \mathbb{C}_{\mathrm{M}}^{\mathrm{GSC}}$ and $f_{\mathcal{S}} = f$. In this case, it means that $c_{\mathcal{S}} = 1$, $c_m = 0$, and the tensor $\mathbb{P}_d^0$ is the Hill tensor for a spherical inclusion. The bulk modulus evaluated from this model is equal to that evaluated from the GMT model (Eq. (27)) and the effective shear modulus is obtained by solving:

$$\mathrm{V}_d(\mu_{\mathrm{M}}^{\mathrm{GSC}})^2 + (\mathrm{R}_d - \mathrm{V}_n)\mu_{\mathrm{M}}^{\mathrm{GSC}} - \mathrm{R}_n = 0 \tag{29}$$

where V_n, V_d, R_n and R_d are expressed in (A.9).

The composite sphere assemblage models (CSA) of Duan et al. (2005b) (only derived for the bulk modulus) can also be directly refound by using the MRP approach. Indeed, these models provide bounds for the effective elastic properties of a generalized Hashin assemblage built with the single pattern $\mathcal{S}$ (without MOP). For such a material, the CSA models of Duan et al. (2005b) are simply the GV and GR bounds obtained from Eqs. (9) and (10):

$$\mathbb{C}_{\mathrm{M}}^{\mathrm{GV}} = \mathbb{C}_{\mathrm{M}\mathcal{S}}^{\mathrm{GV}} \quad \text{and} \quad \mathbb{C}_{\mathrm{M}}^{\mathrm{GV}} = \mathbb{C}_{\mathrm{M}\mathcal{S}}^{\mathrm{GV}} \tag{30}$$

with the tensors $\mathbb{C}_{\mathrm{M}\mathcal{S}}^{\mathrm{GV}}$ and $\mathbb{C}_{\mathrm{M}\mathcal{S}}^{\mathrm{GV}}$ given by Eq. (22) and taking $f_{\mathcal{S}}$ equal to the total porosity f.

The three previous models (GSC estimate, GV and GR bounds) lead to the same effective bulk modulus which is also the bulk modulus obtained from the GMT estimate. The GV and GR bounds being equal, it means that the exact effective bulk modulus for this material has been obtained. Let us remark that the GV and GR bounds for the shear modulus are now available. For building a generalized Hashin assemblage with a single pattern (which is a fractal structure), the members of the pattern must be distinct in size and homothetic (by definition) in order to tessellate the entire domain. However, for the GMT, GSC, GV, and GR models, a characteristic length has been fixed in the pattern (by considering that the interfacial region has zero thickness) and the entire domain is directly built with one pattern. So in these models, all the members of the pattern have the same size and it cannot tessellate, strictly speaking, all the entire domain. By doing so, these models are not representative of a generalized Hashin assemblage built from a single pattern. This difficulty can be overcome by introducing a MOP.

Then the first-order bounds derived by Le Quang and He (2008) (LQH bounds) can also be derived from the MRP approach. Let us consider a material made of a MOP and p patterns $\mathcal{S}^{(i)}$ where the porosity of each pattern, $f_{\mathcal{S}}^{(i)}$, is equal to 1 for all i from 1 to p: it means that the matrix is only in the MOP and that there is no matrix inside the pattern. Each pattern $\mathcal{S}^{(i)}$ has its own interface moduli denoted by $k_s^{(i)}$ and $\mu_s^{(i)}$, its own internal radius $r_1^{(i)}$, and volumic fraction f_i. In this case, the GV and GR bounds can be expressed as:

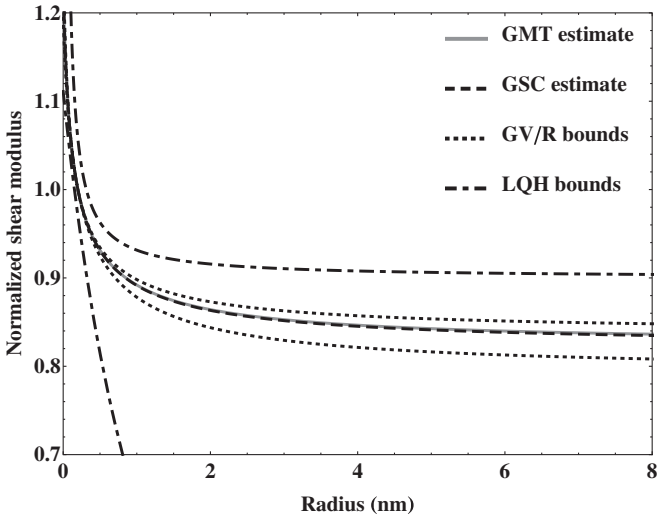

Fig. 3. Effective shear modulus (normalized with respect to the shear modulus of the matrix) as a function of the radius of the cavities. The total porosity f is equal to 5%. The models are evaluated by setting $f_{\mathcal{S}} = f$.

$$\mathbb{C}_{\mathrm{M}}^{\mathrm{GV}} = c_m\mathbb{C}_m + \sum_{i=1}^{i=p} f_i\mathbb{C}_{\mathrm{M}\mathcal{S}^{(i)}}^{\mathrm{GV}} \quad \text{and}$$

$$[\mathbb{C}_{\mathrm{M}}^{\mathrm{GR}}]^{-1} = c_m[\mathbb{C}_m]^{-1} + \sum_{i=1}^{i=p} f_i[\mathbb{C}_{\mathrm{M}\mathcal{S}^{(i)}}^{\mathrm{GR}}]^{-1} \tag{31}$$

where the tensors $\mathbb{C}_{\mathrm{M}\mathcal{S}^{(i)}}^{\mathrm{GV}}$ and $\mathbb{C}_{\mathrm{M}\mathcal{S}^{(i)}}^{\mathrm{GR}}$ are derived from Eq. (22):

$$\mathbb{C}_{\mathrm{M}\mathcal{S}^{(i)}}^{\mathrm{GV}} = \frac{4k_s^{(i)}}{r_1^{(i)}}\mathbb{J} + 2\frac{k_s^{(i)}+6\mu_s^{(i)}}{5r_1^{(i)}}\mathbb{K}$$

$$\mathbb{C}_{\mathrm{M}\mathcal{S}^{(i)}}^{\mathrm{GR}} = \frac{4k_s^{(i)}}{r_1^{(i)}}\mathbb{J} + \frac{10k_s^{(i)}\mu_s^{(i)}}{(6k_s^{(i)}+\mu_s^{(i)})r_1^{(i)}}\mathbb{K} \tag{32}$$

If the stiffness tensor $\mathbb{C}_m$ is isotropic, then the previous bounds match with the bounds of Le Quang and He (2008). Nevertheless, the bounds of Le Quang and He (2008) are not based on the MRP theory but on admissible fields which are uniform in the matrix and in the pores together with the variational principle. In fact, these assumptions are, in this case, in full agreement with those of the GV and GR models. The bounds of Le Quang and He (2008) (for the porous media) appear as a particular case of the GV and GR bounds derived with the patterns $\mathcal{S}^{(i)}$.

In the approach of Le Quang and He (2008), the admissible field over the matrix is fully uniform which is a crude approximation. This is not the case for the GV and GR bounds when the $f_{\mathcal{S}}^{(i)}$ remain free, which implies that an amount of matrix can be taken into account inside each pattern. This would lead to non-uniform fields inside the matrix of the composite and a better description of the heterogeneity of the exact fields inside the composite. Following this idea, it means that it would be more relevant to build bounds based on the GV and GR procedure with a non-zero amount of matrix inside each pattern. This is illustrated in Fig. 3. The GMT, GSC, GV, GR, and LQH models are compared in the case of a porous material with a single mono-sized population of cavities. The models derived from the MRP approach are evaluated by setting $f_{\mathcal{S}}$ to f (no MOP). One should remark that the GMT and GSC estimate are close to each other and they respect the GV and GR bounds. Moreover it appears that the GV and GR bounds improve

the LQH bounds. In the following, the material data used for the numerical implementations are:

- $E_m = 188$ GPa, $\nu_m = 0.3$, for the Young modulus and the Poisson ratio of the matrix. These values are relative to compact UO_2 at 1200^oC following the study of Martin (1989).
- $k_s = 26.85\ N/m$, $\mu_s = 14.46\ N/m$ for the bulk and the shear moduli of the surface. This value for the bulk is in the range of those specified by Wolfer (2011) for Al, Au, and Ag nanoparticles. Unfortunately, to the best of our knowledge, these surface moduli are not known for compact UO_2. Here, the equivalence between the interface and the thin elastic layer of Brisard et al. (2010a) has been used to derive the proposed values for k_s and μ_s: the layer is considered to be 200 times stiffer than the matrix; its thickness is set to 0.001 nm following Le Quang and He (2008) in such a way that it remains smaller than the typical length of the nanocavities.

4. New estimates for nanoporous materials

In this section, two particular cases are considered to illustrate the ability of the MRP approach to extend the existing models: the influence of a spatial distribution of the centers of the voids is investigated, then the case of a bi-porous material containing spherical nanovoids and randomly oriented spheroidal microvoids is considered.

4.1. Ellipsoidal spatial distribution of voids

Unlike the other models, the GMT estimates easily allow us to take into account a spheroidal spatial distribution of the centers of the patterns without defining new patterns with an external shape related to the distribution. Here the material is assumed to be composed of mono-sized voids. Thus the GMT estimate is still derived from Eq. (26). As already stated for this kind of model, one can impose $f_{\mathcal{S}} = 1$ without loss of generality (it implies that $f = c_{\mathcal{S}}$). The Hill tensor $\mathbb{P}_d^m$ is then related to the spheroidal distribution and is expressed by Eq. (15) in terms of the Eshelby tensor $\mathbb{S}^E(\mathbb{C}_m)$. Denoting by a and b the semi-length of the vertical (z axis) and the horizontal axes of the spheroid (ellipsoid which is rotation invariant around the z axis) the spheroidal distribution aspect-ratio is expressed as:

$$\omega_d = a/b \tag{33}$$

The overall material presents a transversely isotropic symmetry with respect to the z axis. The effective stiffness tensor can be put under the following form:

$$\mathbb{C}_{\mathrm{M}}^{\mathrm{GMT}} = n\mathbb{E}_l + 2k_t\mathbb{J}_t + \sqrt{2}l(\mathbb{F} + {}^{\mathrm{T}}\mathbb{F}) + 2\mu_t\mathbb{K}_t + 2\mu_l\mathbb{K}_l \tag{34}$$

where $\mathbb{E}_l$, $\mathbb{J}_t$, $\mathbb{F}$, ${}^{\mathrm{T}}\mathbb{F}$, $\mathbb{K}_t$ and $\mathbb{K}_l$ are the basis tensors for fourth-order transversely isotropic tensors defined in Suquet and Bornert (2001).

The Figs. 4 and 5 show the evolutions of the effective elastic constants as a function of the aspect ratio ω_d for an oblate ($a < b$) and a prolate ($a > b$) spheroidal spatial distribution of the centers[4]. The radius of the voids is set to $r_1 = 1$ nm. The total porosity is set to an artificially large value $f = 25$ % in order to enhance the effect of the voids. The effective elastic constants are normalized with respect to the effective elastic constants when the spatial distribution is isotropic ($\omega_d = 1$). The following observations can be made:

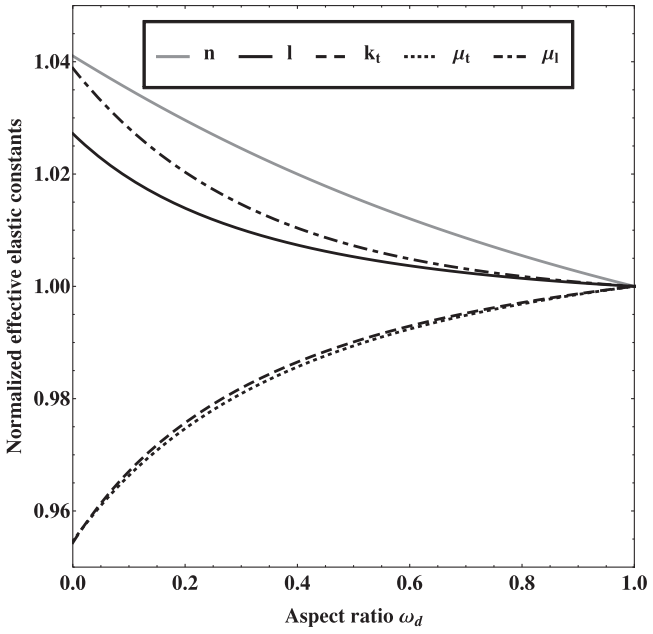

Fig. 4. Effective elastic constants as a function of the aspect ratio for an oblate spheroidal spatial distribution of the centers of the pattern $\mathcal{S}$. The total porosity f is equal to 25% and the radius of the voids is 1 nm.

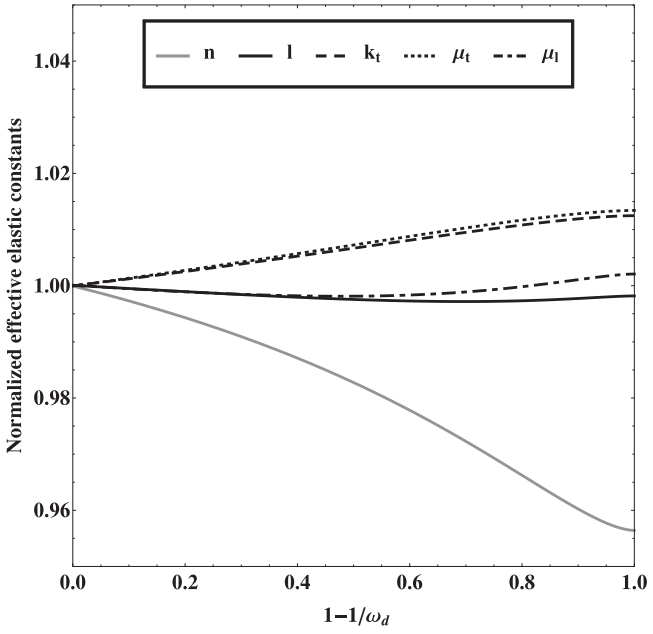

Fig. 5. Effective elastic constants as a function of the aspect ratio for a prolate spheroidal spatial distribution of the centers of the pattern $\mathcal{S}$. The total porosity f is equal to 25% and the radius of the voids is 1 nm.

- first, one can observe that the overall behavior becomes more anisotropic when ω_d tends to 0 (oblate case) and when $1 - 1/\omega_d$ tends to 1 (prolate case): the difference between the longitudinal coefficients (n, μ_l) and the transverse coefficients (k_t, μ_t) increases when ω_d tends to these particular values.
- in the oblate case, the longitudinal coefficients (n, μ_l) become stiffer when ω_d tends to 0 and the transverse coefficients become softer compared to the isotropic case ($\omega_d = 1$).
- in the prolate case, only the coefficient n becomes softer when ω_d tends to infinity whereas the coefficients μ_l, k_t, μ_t become stiffer compared to the isotropic case ($\omega_d = 1$).

[4] For prolate spheroid, the evolution of the effective elastic constants is plotted as a function of $1 - 1/\omega_d$ to browse all the range of the possible values of the aspect-ratio.

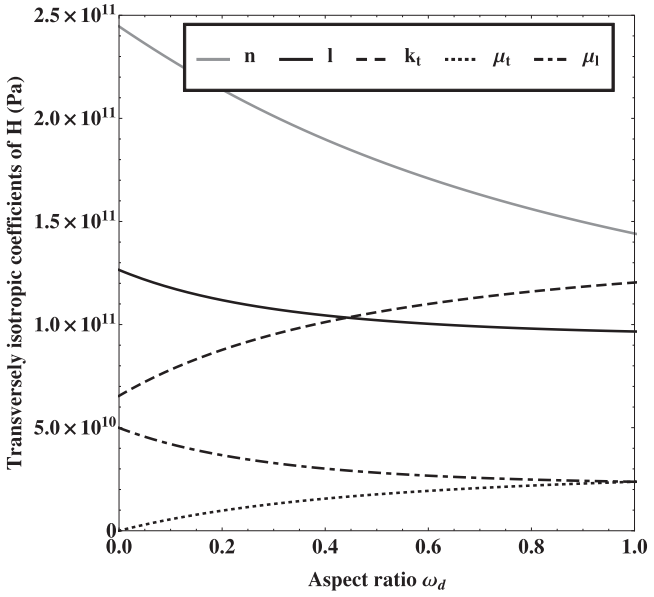

Fig. 6. Transversely isotropic constants of $\mathbb{H}$ as a function of the aspect ratio for an oblate spheroidal spatial distribution of the centers of the pattern $\mathcal{S}$. The total porosity f is equal to 25 % and the radius of the voids is 1 nm.

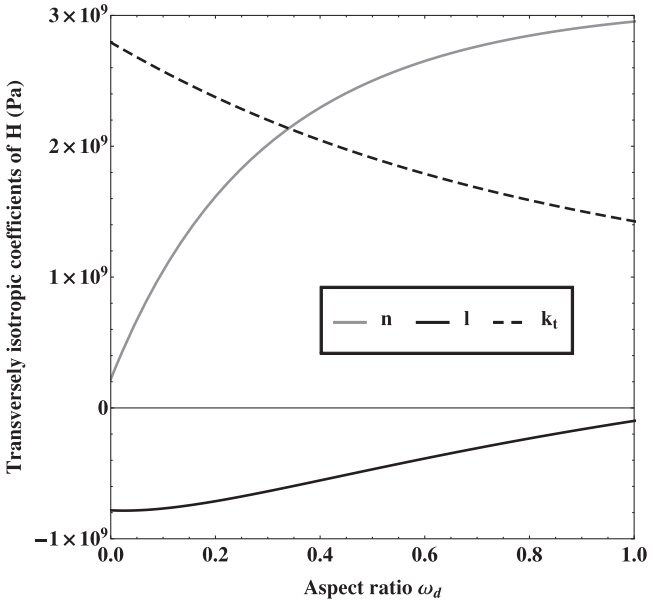

Fig. 7. Transversely isotropic constants of $\mathbb{H}$ as a function of the aspect ratio for an oblate spheroidal spatial distribution of the centers of the pattern $\mathcal{S}$. The total porosity f is equal to 25 % and the radius of the voids is 1 nm. Specific case where $E_m = 100$ GPa, $\nu_m = 0.2$, $k_s = 50$ N/m, $\mu_s = 30$ N/m.

The physical meaning of the two previous items is tricky because of the various effects taken into account in the model. First, the interface induces more stiffness for the overall behavior whereas the void phase induces softening. Secondly, the spatial distribution of the centers of the patterns induces changes in the distances between the cavities and their interactions: for example, when ω_d tends to 0, the spherical voids are spaced far away from each other in the transverse plane and they tend to line up in the axial direction (as already pointed out by Ponte Castañeda and Willis (1995) in the case of rigid particles or cracks). Thirdly, the differences in the behaviors between the matrix and the interface can also influence the overall behavior. To see the influence of the distribution of the centers on the overall behavior, one can write the following Taylor expansion due to Ponte Castañeda and Willis (1995):

$$\mathbb{C}_{\mathrm{M}}^{\mathrm{GMT}} = \mathbb{C}_m + c_{\mathcal{S}}\mathbb{T}_{\mathrm{M}\mathcal{S}}^m + (c_{\mathcal{S}}\mathbb{T}_{\mathrm{M}\mathcal{S}}^m) : \mathbb{P}_d^m : (c_{\mathcal{S}}\mathbb{T}_{\mathrm{M}\mathcal{S}}^m) + O[(c_{\mathcal{S}})^3] \qquad (35)$$

It appears that the shape of the distribution affects $\mathbb{C}_{\mathrm{M}}^{\mathrm{GMT}}$ through the Hill tensor $\mathbb{P}_d^m$ to second order in the volume fraction of the pattern. Let us introduce a new tensor called the first distribution effect tensor as:

$$\mathbb{H} = \mathbb{T}_{\mathrm{M}\mathcal{S}}^m : \mathbb{P}_d^m : \mathbb{T}_{\mathrm{M}\mathcal{S}}^m \qquad (36)$$

The evolution of this $\mathbb{H}$ tensor can be used for studying the specific evolutions of the parameters n, μ_l, k_t, μ_t shown in Figs. 4 and 5. Fig. 6 illustrates the evolution of the transversely isotropic coefficients of $\mathbb{H}$ with respect to ω_d in the oblate case. One can observe that the transverse coefficients of $\mathbb{H}$ (resp. the longitudinal) decreases (resp. increases) when ω_d tends to 0 (aligned case). This is in accordance with the evolutions of the transversely isotropic coefficients of $\mathbb{C}_{\mathrm{M}}^{\mathrm{GMT}}$ shown in Fig. 4. When ω_d tends to 0, the spherical voids are spaced far away from each other in the transverse plane. It may be understood that the interactions between the voids decrease in the transverse plane which could lead to softer transverse coefficients. On the other hand, it implies that the voids are spaced close to each other in the longitudinal direction. Therefore, the interactions between the voids may increase in this direction which could lead to stiffer longitudinal coefficients. It is also possible to demonstrate that the transverse shear of the $\mathbb{H}$ tensor is zero when ω_d tends to 0 (aligned case). It means that, in this case and for the transverse shear of $\mathbb{C}_{\mathrm{M}}^{\mathrm{GMT}}$, the voids are so far from each other that the interaction effect is neglectable and the model reduces to the dilute case.

Moreover it has been shown that the longitudinal shear (resp. the transverse shear) coefficient for the difference $\mathbb{H}(\omega_d = 0) - \mathbb{H}(\omega_d = 1)$ is still positive (resp. negative) for all the values of the other coefficients (matrix and interface coefficients, radius of the voids). It implies that the overall longitudinal shear (resp. the overall transverse shear) predicted by the model will be still stiffer (resp. softer) in the aligned case ($\omega_d = 0$) than in the isotropic case ($\omega_d = 1$).

The same conclusion cannot be generalized to the other coefficients (n, l, k_t) of $\mathbb{C}_{\mathrm{M}}^{\mathrm{GMT}}$. It is illustrated in Fig. 7, where the $\mathbb{H}$ tensor exhibits another trend for its transversely isotropic coefficients (n, l, k_t), for other choices of the parameters ($E_m = 100$ GPa, $\nu_m = 0.2$, $k_s = 50$ N/m , $\mu_s = 30$ N/m).

4.2. A second population of cavities

Let us consider now the case of a bi-porous material. The first population of voids is assumed to be composed of nano-spherical voids and the second population is assumed to be composed of spheroidal (more precisely oblate) voids whose the size is larger enough to avoid the surface effects. The spatial distribution of the centers of the voids is assumed to be isotropic. As already stated in the introduction, such a microstructure is representative of the irradiated UO_2. Indeed, this material contains intragranular cavities, almost spherical in shape with a typical diameter of a few nanometers, and at a larger scale, intergranular cavities, roughly ellipsoidal in shape with a typical size of a few microns and located at the grain boundaries (see for example (Vincent et al., 2008; Vincent et al., 2009a; Vincent et al., 2014a)).

Two patterns have to be specified: (i) a pattern for the spherical nanovoids (we make use of the already defined pattern $\mathcal{S}$), (ii) a pattern denoted by $\mathcal{E}$ made of a spheroidal oblate microvoid (without surface effect). The major axis of the ellipsoidal cavity are denoted by a and b and the aspect ratio ω is equal to a/b. The auxiliary problem related to the pattern $\mathcal{E}$ is a classical Eshelby inclusion problem (where the inclusion is a void). The total porosity

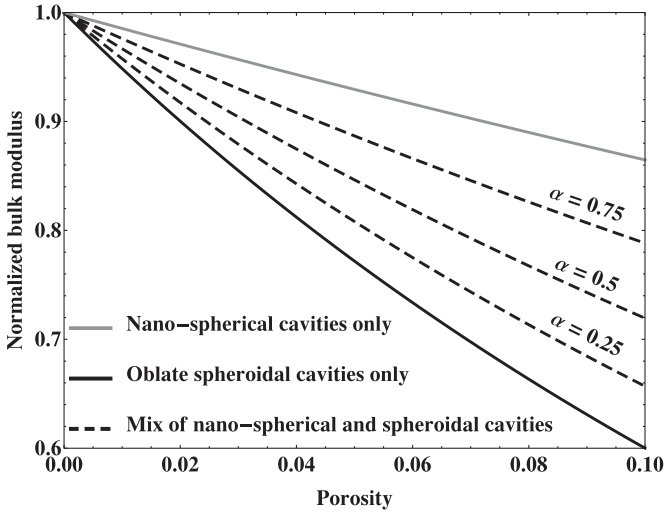

Fig. 8. Normalized effective bulk modulus as a function of the total porosity. Aspect ratio of the microvoids $\omega = 0.2$. Radius of the spherical nanovoids $r = 1$ nm.

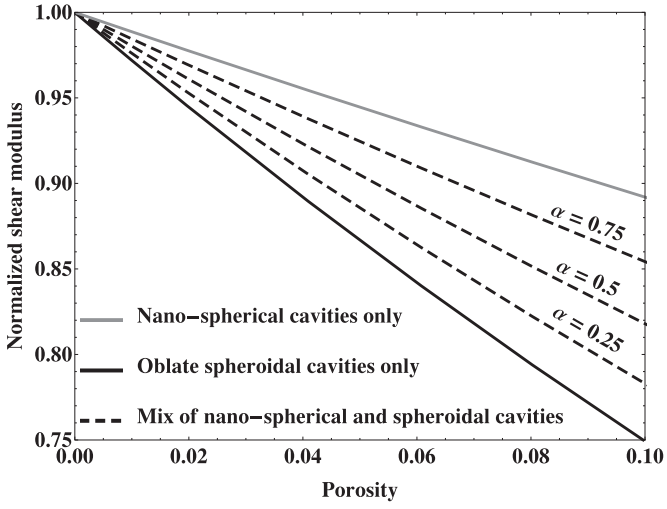

Fig. 9. Normalized effective shear modulus as a function of the total porosity. Aspect ratio of the microvoids $\omega = 0.2$. Radius of the spherical nanovoids $r = 1$nm.

is denoted by f. The porosity of the nano-spherical voids is equal to αf and the porosity of spheroidal voids is equal to $(1-\alpha)f$ where α is a parameter, ranging from 0 to 1. The GMT estimate is derived from (14):

$$\langle \mathbb{T}^m_{\mathrm{Mr}} \rangle_{\mathrm{M}} = \alpha f \mathbb{T}^m_{\mathrm{M}\mathcal{S}} + (1-\alpha) f \langle \mathbb{T}^m_{\mathcal{E}} \rangle_{\circlearrowleft} \tag{37}$$

The operator $\langle . \rangle_{\circlearrowleft}$ denotes an average over all the orientations. The tensor $\mathbb{T}^m_{\mathcal{E}}$ is the classical tensor for an ellipsoidal cavity without surface effect:

$$\mathbb{T}^m_{\mathcal{E}} = -\mathbb{C}_m : (\mathbb{C}^\star_m)^{-1} : (\mathbb{C}^\star_m + \mathbb{C}_m) \tag{38}$$

with $\mathbb{C}^\star_m = \mathbb{P}^{-1}_m - \mathbb{C}_m$ and $\mathbb{P}_m = \mathbb{S}^E(\mathbb{C}_m) : \mathbb{C}^{-1}_m$. The tensor $\mathbb{S}^E(\mathbb{C}_m)$ is the Eshelby tensor relative to the shape of the oblate voids when the matrix is the reference medium. Then according to Gatt et al. (2005), the average can be expressed as:

$$\langle \mathbb{T}^m_{\mathcal{E}} \rangle_{\circlearrowleft} = \left(\mathbb{T}^m_{\mathcal{E}} :: \mathbb{J} \right) + \frac{1}{5} \left(\mathbb{T}^m_{\mathcal{E}} :: \mathbb{K} \right) \tag{39}$$

The evolution of the effective moduli (normalized with respect to the matrix moduli) as a function of the total porosity is illustrated in Figs. 8 and 9. From these figures, one can observe that the relative difference for the effective bulk moduli, between the case where all the porosity corresponds to oblate microvoids and the case where all the porosity corresponds to spherical nanovoids, is about 20 % when the porosity reaches 5 % which is a common value for the porosity in irradiated UO_2. A similar trend can be observed for the effective shear modulus.

5. Conclusion

This study is devoted to the modeling of the elastic behavior of porous media with spherical nanovoids. It is shown here that the existing models can be directly derived following the Morphologically Representative Pattern (MRP) approach of Stolz and Zaoui (1991). Several particular cases have been considered to illustrate the ability of the MRP approach to extend the existing estimates and bounds. First the influence of a spatial distribution of the centers of the voids has been investigated, showing a complex dependence of the elastic moduli with respect to the material and geometric parameters. A new model has been proposed for dealing with an ellipsoidal spatial distribution of the voids. It has been checked that, for an isotropic spatial distribution, the proposed model reduces to the model of Duan et al. (2005b). Then the case of a bi-porous material containing spherical nanovoids and randomly oriented spheroidal microvoids has been treated. This result is of a great interest for modeling the elastic behavior of biporous materials such as the irradiated uranium dioxide. This work proves that the MRP approach can be easily applied to complex microstructures such as nanovoids together with different kinds of heterogeneities.

Appendix A. Auxiliary problem

The auxiliary problem relative to the pattern $\mathcal{S}$ (Section 3.2) is defined as a spherical cavity (radius r_1) surrounded by a matrix layer (index m, radius r_0). This domain is embedded in an infinite homogeneous medium (reference medium, index 0) submitted to a remote strain $\boldsymbol{\epsilon}^0$ applied at infinity. The interface stress model is applied at the interface between the void and the matrix.

A1. Hydrostatic loading

First, an hydrostatic remote strain $\boldsymbol{\epsilon}^0 = \epsilon^0_h \boldsymbol{i}$ is applied. The displacement field and stress vector in each phases have the following forms (in the spherical coordinates system):

$$\begin{aligned} &\forall i \in \{m, 0\}, \quad \boldsymbol{u}^{(i)} = \left(A_i r + \frac{B_i}{r^2} \right) \boldsymbol{e_r} \quad \text{and} \\ &\boldsymbol{\sigma}^{(i)} \cdot \boldsymbol{n} = \left(3k_i A_i - \frac{4\mu_i B_i}{r^3} \right) \boldsymbol{e_r} \end{aligned} \tag{A.1}$$

The four constants, A_0, B_0, A_m and B_m have to be determined by using the boundary conditions. For the displacement field in the reference medium at infinity, it comes that $A_0 = \epsilon^0_h$. Then, the three other constants are obtained from the continuity of the stress vector at Γ_0, the continuity of the displacement at Γ_0, and the equilibrium conditions of the imperfect coherent interface at Γ_1.

Then the average of the stress and strain fields over the pattern $\mathcal{S}$ can be easily expressed and it comes that:

$$\begin{cases} T^0_{\mathrm{M}\mathcal{S}|h} = \dfrac{(3k_0 + 4\mu_0)(4\alpha_h - 3k_0\beta_h)}{4\gamma_h} \\ k^{\mathrm{HS}}_{\mathrm{M}\mathcal{S}} = \dfrac{4}{3} \dfrac{3k_m\mu_m(1-f_S)r_1 + k_s(3k_m + 4f_S\mu_m)}{(3f_S k_m + 4\mu_m)r_1 + 4(1-f_S)k_s} \end{cases} \tag{A.2}$$

$$\begin{cases} \alpha_h = k_s(4f_S\mu_m + 3k_m) + 3(1-f_S)k_m\mu_m r_1 \\ \beta_h = 4(1-f_S)k_s + r_1(3f_S k_m + 4\mu_m) \\ \gamma_h = k_s(4((1-f_S)\mu_0 + f_S\mu_m) + 3k_m) \\ \qquad + r_1(3f_S k_m(\mu_0 - \mu_m) + \mu_m(3k_m + 4\mu_0)) \end{cases} \tag{A.3}$$

Particularly, when the reference medium is the matrix, it comes that:

$$T^{m}_{\mathrm{M}\mathcal{S}|h} = f_{\mathcal{S}}\frac{(3k_m+4\mu_m)(4k_s-3k_m r_1)}{4(k_s+\mu_m r_1)} \tag{A.4}$$

The scalar $f_{\mathcal{S}} = (r_1/r_0)^3$ corresponds to the porosity of the pattern $\mathcal{S}$.

A2. Deviatoric loading

Then a deviatoric remote strain is applied (in the Cartesian coordinates system):

$$\boldsymbol{\epsilon}^0 = -\gamma\,(\boldsymbol{e_x}\otimes\boldsymbol{e_x} + \boldsymbol{e_y}\otimes\boldsymbol{e_y} - 2\boldsymbol{e_z}\otimes\boldsymbol{e_z}) \tag{A.5}$$

In each phase ($\forall i \in \{m, 0\}$), the displacement and stress vector fields are (ν_i refers to Poisson ratios):

$$\begin{aligned}\boldsymbol{u}^{(i)} = &-\left(A_i r + B_i r^3 + \frac{C_i}{r^2} + \frac{D_i}{r^4}\right)\left(1-3\cos^2(\theta)\right)\boldsymbol{e_r}\\ &-\left(3A_i r + \frac{(7-4\nu_i)r^3}{2\nu_i}B_i + \frac{6(1-2\nu_i)}{(5-4\nu_i)r^2}C_i - \frac{2}{r^4}D_i\right)\\ &\times\cos(\theta)\sin(\theta)\boldsymbol{e_\theta}\end{aligned} \tag{A.6}$$

$$\begin{aligned}\frac{\boldsymbol{\sigma}^{(i)}\cdot\boldsymbol{n}}{\mu_i} = &\left(A_i - \frac{1}{2}r^2 B_i - \frac{2(5-\nu_i)}{(5-4\nu_i)r^3}C_i - \frac{4}{r^5}D_i\right)\left(1+3\cos(2\theta)\right)\boldsymbol{e_r}\\ &-\left(6A_i + \frac{(7+2\nu_i)r^2}{\nu_i}B_i + \frac{12(1+\nu_i)}{(5-4\nu_i)r^3}C_i + \frac{16}{r^5}D_i\right)\\ &\times\cos(\theta)\sin(\theta)\boldsymbol{e_\theta}\end{aligned} \tag{A.7}$$

The eight constants A_0, B_0, C_0, D_0, A_m, B_m, C_m and D_m have to be determined. The remote strain imposes that $A_0 = \gamma$ and $B_0 = 0$. The six other constants are obtained from the continuity of displacement field components u_r and u_θ at Γ_0, the continuity of the stress field components σ_{rr} and $\sigma_{r\theta}$ at Γ_0, and the equilibrium of the imperfect coherent interface at Γ_1. The averages of the stress and strain fields over the pattern $\mathcal{S}$ can then be derived. Then the deviatoric parts of the tensors $\mathbb{T}^0_{\mathrm{M}\mathcal{S}}$ and $\mathbb{C}^{\mathrm{HS}}_{\mathrm{M}\mathcal{S}}$ read:

$$T^0_{\mathrm{M}\mathcal{S}|d} = -10\frac{3k_0+4\mu_0}{15(k_0+\mu_0)r_0^3}\mu_0\frac{C_0}{\gamma} \quad\text{and}\quad \mu^{\mathrm{HS}}_{\mathrm{M}\mathcal{S}} = \frac{\mathrm{R}_n+\mathrm{V}_n\mu_0}{\mathrm{R}_d+\mathrm{V}_d\mu_0} \tag{A.8}$$

The constants R_n, R_d, V_n and V_d depend on the material properties and the geometry (k_m, μ_m, k_s, μ_s, r_0 and r_1) but do not depend on the elastic properties of the reference medium. Moreover, they are polynomials of the second degree in terms of r_1 and they can be written as $\mathrm{R}_n = \mathrm{A}(3,1)$, $\mathrm{R}_d = \mathrm{A}(4,2)$, $\mathrm{V}_n = \mathrm{A}(1,2)$, $\mathrm{V}_d = \mathrm{A}(2,3)$ with:

$$\mathrm{A}(i,j) = \sum_{k=1}^{3} f_k(i,j) r_1^{k-1} \tag{A.9}$$

The functions $f_k(i,j)$ (with $k \in [1,\ldots,3]$) have the following forms:

$$\begin{aligned} f_1(i,j) &= k_s\mu_s\mu_m^{3-j}\xi\left(\mathrm{M}_1^{(i)},\mathrm{M}_2^{(i)},\mathrm{M}_3^{(i)}\right)\\ f_2(i,j) &= \mu_m^{4-j}\left[k_s\xi\left(\mathrm{M}_4^{(i)},\mathrm{M}_5^{(i)},\mathrm{M}_6^{(i)}\right) + \mu_s\xi\left(\mathrm{M}_7^{(i)},\mathrm{M}_8^{(i)},\mathrm{M}_9^{(i)}\right)\right]\\ f_3(i,j) &= \mu_m^{5-j}\xi\left(\mathrm{M}_{10}^{(i)},\mathrm{M}_{11}^{(i)},\mathrm{M}_{12}^{(i)}\right)\end{aligned} \tag{A.10}$$

where

$$\xi(x,y,z) = k_m^2 x + k_m\mu_m y + \mu_m^2 z \tag{A.11}$$

The coefficients $M_j^{(i)}$, ($\forall i \in [1,\ldots,4]$, $\forall j \in [1,\ldots,12]$) depend only on the porosity of the pattern $f_{\mathcal{S}} = (r_1/r_0)^3$ and can be written as:

$$\mathrm{M}_j^{(i)} = a_j^{(i)} + b_j^{(i)} f_{\mathcal{S}} + c_j^{(i)} f_{\mathcal{S}}^{5/3} + d_j^{(i)} f_{\mathcal{S}}^{7/3} + e_j^{(i)} f_{\mathcal{S}}^{10/3} \tag{A.12}$$

Table A1
Coefficients $a_j^{(1)}$, $b_j^{(1)}$, $c_j^{(1)}$, $d_j^{(1)}$, and $e_j^{(1)}$ ($\forall j \in [1,\ldots,12]$).

j	$a_j^{(1)}$	$b_j^{(1)}$	$c_j^{(1)}$	$d_j^{(1)}$	$e_j^{(1)}$
1	−288	1080	−3024	1800	432
2	−1392	−600	−2016	2400	1608
3	−1632	−920	−336	1800	1088
4	−576	−1080	1512	450	−621
5	−2208	600	−504	3300	−2028
6	−1632	920	−336	1800	−1312
7	−432	1080	−4536	2700	−702
8	−1992	−600	−4536	3000	−912
9	−2176	−920	−1008	1000	−256
10	−432	−1080	3024	−2025	513
11	−1608	600	2016	−1500	492
12	−1088	920	336	−200	32

Table A2
Coefficients $b_j^{(2)}$, $e_j^{(2)}$, $a_j^{(3)}$, $b_j^{(3)}$, and $b_j^{(4)}$ ($\forall j \in [1,\ldots,12]$).

j	$b_j^{(2)}$	$e_j^{(2)}$	$a_j^{(3)}$	$b_j^{(3)}$	$b_j^{(4)}$
1	1800	−288	−342	−2025	−1170
2	2400	−1392	−708	−1500	−300
3	1800	−1632	−48	−200	−120
4	−1800	414	−684	2025	1170
5	−2400	1812	−732	1500	300
6	−1800	1968	−48	200	120
7	1800	468	−513	−2025	−1170
8	2400	1128	−948	−1500	−300
9	1800	384	−64	−200	−120
10	−1800	−342	−513	2025	1170
11	−2400	−708	−492	1500	300
12	−1800	−48	−32	200	120

where the coefficients $a_j^{(i)}$, $b_j^{(i)}$, $c_j^{(i)}$, $d_j^{(i)}$, and $e_j^{(i)}$ ($\forall i \in [1,\ldots,4]$, $\forall j \in [1,\ldots,12]$) are obtained from Tables A.1 and A.2, with the following relations:

$$\begin{aligned}\forall j \in [1,\ldots,12],\quad & a_j^{(2)} = a_j^{(1)},\quad a_j^{(3)} = a_j^{(4)},\\ & c_j^{(2)} = c_j^{(1)} = -c_j^{(3)} = -c_j^{(4)},\\ & d_j^{(2)} = d_j^{(1)} = -d_j^{(3)} = -d_j^{(4)},\\ & e_j^{(3)} = -e_j^{(1)},\quad e_j^{(4)} = -e_j^{(2)}\end{aligned} \tag{A.13}$$

The expression of C_0/γ (in (A.8)) does not depend on γ, and then the expressions of $\mathbb{T}^0_{\mathrm{M}\mathcal{S}}$ does not depend on the amplitude of the external loading. Its expression can easily be derived using (11) and (12):

$$\frac{C_0}{\gamma} = r_0^3\frac{15(k_0+\mu_0)(\mu_0-\mu^{\mathrm{HS}}_{\mathrm{M}\mathcal{S}})}{(9k_0+8\mu_0)\mu_0 + 6\mu^{\mathrm{HS}}_{\mathrm{M}\mathcal{S}}(k_0+2\mu_0)} \tag{A.14}$$

Unlike the effective bulk modulus $k^{\mathrm{HS}}_{\mathrm{M}\mathcal{S}}$, the shear modulus $\mu^{\mathrm{HS}}_{\mathrm{M}\mathcal{S}}$ depends on the stiffness $\mathbb{C}_0$ (only on μ_0). From this remark and Eq. (13), it comes:

$$\mu^{\mathrm{GV}}_{\mathrm{M}\mathcal{S}} = \frac{\mathrm{V}_n}{\mathrm{V}_d} \quad\text{and}\quad \mu^{\mathrm{GR}}_{\mathrm{M}\mathcal{S}} = \frac{\mathrm{R}_n}{\mathrm{R}_d} \tag{A.15}$$

Let us remark that, when the reference medium is the matrix, it comes that:

$$\begin{cases} T^m_{\mathrm{M}\mathcal{S}|d} = f_{\mathcal{S}}\dfrac{10\mu_m(3k_m+4\mu_m)\beta_d}{3k_m\delta_d+4\mu_m\zeta_d}\\ \beta_d = (k_s+r_1\mu_m)(\mu_s-r_1\mu_m)\\ \delta_d = 3r_1\mu_m(r_1\mu_m+\mu_s)+2k_s(2r_1\mu_m+\mu_s)\\ \zeta_d = 3k_s(r_1\mu_m+\mu_s)+2r_1\mu_m(r_1\mu_m+2\mu_s)\end{cases} \tag{A.16}$$

References

Bornert, M., 1996a. A generalized pattern-based self-consistent scheme. Comput. Mater. Sci. 5 (1-3), 17–31.

Bornert, M., 1996b. Morphologie microstructurale et comportement mécanique; caractérisations expérimentales, approches par bornes et estimations autocohérentes généralisées. (Ph.D. thesis). Ecole Nationale des Ponts et Chaussées.

Bornert, M., 2001. Homogénéisation des milieux aléatoires : bornes et estimations. In: Bornert, M., Bretheau, T., Gilormini, P. (Eds.), Homogénéisation en mécanique des matériaux, 1. Hermès Science Publications, Paris, pp. 133–221.(chapter 5)

Bornert, M., Stolz, C., Zaoui, A., 1996. Morphologically representative pattern based bounding in elasticity. J. Mech. Phys. Solids 44 (3), 307–330.

Brisard, S., Dormieux, L., Kondo, D., 2010a. Hashin–Shtrikman bounds on the bulk modulus of a nanocomposite with spherical inclusions and interface effects. Comput. Mater. Sci. 48 (3), 589–596.

Brisard, S., Dormieux, L., Kondo, D., 2010b. Hashin–Shtrikman bounds on the shear modulus of a nanocomposite with spherical inclusions and interface effects. Comput. Mater. Sci. 50 (2), 403–410.

Christensen, R., Lo, K., 1979. Solutions for effective shear properties in three phase sphere and cylinder models. J. Mech. Phys. Solids 27 (4), 315–330.

Duan, H., Wang, J., Huang, Z., Karihaloo, B., 2005a. Eshelby formalism for nano-inhomogeneities. Proc. R. Soc. A: Math., Phys. Eng. Sci. 461 (2062), 3335–3353.

Duan, H., Wang, J., Huang, Z., Karihaloo, B., 2005b. Size-dependent effective elastic constants of solids containing nano-inhomogeneities with interface stress. J. Mech. Phys. Solids 53 (7), 1574–1596.

Duan, H., Wang, J., Huang, Z., Luo, Z., 2005c. Stress concentration tensors of inhomogeneities with interface effects. Mech. Mater. 37 (7), 723–736.

Duan, H., Wang, J., Karihaloo, B., Huang, Z., 2006. Nanoporous materials can be made stiffer than non-porous counterparts by surface modification. Acta Mater. 54 (11), 2983–2990.

Duan, H., Yi, X., Huang, Z., Wang, J., 2007. A unified scheme for prediction of effective moduli of multiphase composites with interface effects. Part I: Theoretical framework. Mech. Mater. 39 (1), 81–93.

Eshelby, J.D., 1957. The determination of the elastic field of an ellipsoidal inclusion, and related problem. Proc. R. Soc. Lond. A 241, 376–396.

Gatt, J.-M., Monerie, Y., Laux, D., Baron, D., 2005. Elastic behavior of porous ceramics: Application to nuclear fuel materials. J. Nucl. Mater. 336 (2-3), 145–155.

Gurtin, M., Murdoch, A., 1975. A continuum theory of elastic material surfaces. Arch. Ration. Mech. Anal. 57 (4), 291–323.

Hashin, Z., 1962. The elastic moduli of heterogeneous materials. J. Appl. Mech. 29, 143–150.

Huang, Z., Wang, J., 2006. A theory of hyperelasticity of multi-phase media with surface/interface energy effect. Acta Mech. 182 (3-4), 195–210.

Jelea, A., Colbert, M., Ribeiro, F., Tréglia, G., Pellenq, R.-M., 2011. An atomistic modelling of the porosity impact on UO_2 matrix macroscopic properties. J. Nucl. Mater. 415 (2), 210–216.

Julien, J., Gărăjeu, M., Michel, J.-C., 2011. A semi-analytical model for the behavior of saturated viscoplastic materials containing two populations of voids of different sizes. Int. J. Solids Struct. 48, 1485–1498.

Kashibe, S., Une, K., Nogita, K., 1993. Formation and growth of intragranular fission gas bubbles in UO_2 fuels with burnup of 6 – 83 GWd/t. J. Nucl. Mater. 206, 22–34.

Le Quang, H., He, Q.-C., 2008. Variational principles and bounds for elastic inhomogeneous materials with coherent imperfect interfaces. Mech. Mater. 40 (10), 865–884.

Marcadon, M., 2005. Effets de taille et d'interphase sur le comportement mécanique de nanocomposites particulaires. Ecole Polytechnique (Ph.D. thesis).

Martin, D., 1989. The elastic constants of polycrystalline UO_2 and (U,Pu) mixed oxides : a review and recommendations. High Temp.-High Press. 21, 13–24.

Mori, T., Tanaka, K., 1973. Average stress in matrix and average elastic energy of materials with misfitting inclusions. Acta Metall. 21 (5), 571–574.

Paliwal, B., Cherkaoui, M., 2012. Estimation of anisotropic elastic properties of nanocomposites using atomistic-continuum interphase model. Int. J. Solids Struct. 49 (18), 2424–2438.

Ponte Castañeda, P., Willis, J., 1995. The effect of spatial distribution on the effective behavior of composite materials and cracked media. J. Mech. Phys. Solids 43 (12), 1919–1951.

Ru, C., 2010. Simple geometrical explanation of Gurtin-Murdoch model of surface elasticity with clarification of its related versions. Sci. China: Phys., Mech. Astron. 53 (3), 536–544.

Sharma, P., Ganti, S., 2004. Size-dependent Eshelby's tensor for embedded nano-inclusions incorporating surface/interface energies. Trans. ASME J. Appl. Mech., 71 (5), 663–671.

Stolz, C., Zaoui, A., 1991. Analyse morphologique et approches variationnelles du comportement d'un milieu élastique hétérogène.. Comptes Rendus de l'Académie des Sci. 312, 143–150.

Suquet, P., Bornert, M., 2001. Rappels de calcul tensoriel et d'élasticité. In: Bornert, M., Bretheau, T., Gilormini, P. (Eds.), Homogénéisation en mécanique des matériaux, 2. Hermès Science Publications, Paris, pp. 171–202.chapter 5

Vincent, P.-G., Monerie, Y., Suquet, P., 2008. Ductile damage of porous materials with two populations of voids. Comptes Rendus – Mecanique 336 (1-2), 245–259.

Vincent, P.-G., Monerie, Y., Suquet, P., 2009a. Porous materials with two populations of voids under internal pressure: I. Instantaneous constitutive relations. Int. J. Solids Struct. 46, 480–506.

Vincent, P.-G., Monerie, Y., Suquet, P., 2009b. Porous materials with two populations of voids under internal pressure: II. Growth and coalescence of voids. Int. J. Solids Struct. 46, 507–526.

Vincent, P.-G., Suquet, P., Monerie, Y., Moulinec, H., 2014a. Effective flow surface of porous materials with two populations of voids under internal pressure: I. A GTN model. Int. J. Plast. 56, 45–73.

Vincent, P.-G., Suquet, P., Monerie, Y., Moulinec, H., 2014b. Effective flow surface of porous materials with two populations of voids under internal pressure: II. Full-field simulations. Int. J. Plast. 56, 74–98.

Wang, J., Duan, H., Zhang, Z., Huang, Z., 2005. An anti-interpenetration model and connections between interphase and interface models in particle-reinforced composites. Int. J. Mech. Sci. 47 (4-5), 701–718.

Wang, J., Huang, Z., Duan, H., Yu, S., Feng, X., Wang, G., Zhang, W., Wang, T., 2011. Surface stress effect in mechanics of nanostructured materials. Acta Mech. Solida Sinica 24 (1), 52–82.

Wang, J., Karihaloo, B., Duan, H., 2007. Nano-mechanics or how to extend continuum mechanics to nano-scale. Bull. Pol. Acad. Sci.: Tech. Sci. 55 (2), 133–140.

Wolfer, W., 2011. Elastic properties of surfaces on nanoparticles. Acta Mater. 59 (20), 7736–7743.